tvst

Lens

Assessment of Diffractive Intraocular Lenses Using Near-Infrared Light: A Critical Evaluation

Ricardo Elsner[1,2], Mario Gerlach[3], Sebastian Bohn[1,2], Jan Sievers[4], Heinrich Stolz[5], Rudolf F. Guthoff[1,2], Oliver Stachs[1,2], and Karsten Sperlich[1,2]

[1] Department of Ophthalmology, Rostock University Medical Center, Rostock, Germany
[2] Department Life, Light & Matter, University of Rostock, Rostock, Germany
[3] Carl Zeiss Meditec AG, ZEISS Group, Berlin, Germany
[4] Institute of Physics, Martin–Luther–University Halle–Wittenberg, Halle (Saale), Germany
[5] Institute of Physics, University of Rostock, Rostock, Germany

Correspondence: Ricardo Elsner, Department of Ophthalmology, Rostock University Medical Center, Doberaner Str. 140, Rostock 18057, Germany. e-mail: elsner.ricardo@gmail.com or ricardo.elsner@charite.de

Received: December 13, 2024
Accepted: May 15, 2025
Published: June 30, 2025

Keywords: NIR light; diffractive IOL; MIOL; optical bench; wavefront aberrometer

Citation: Elsner R, Gerlach M, Bohn S, Sievers J, Stolz H, Guthoff RF, Stachs O, Sperlich K. Assessment of diffractive intraocular lenses using near-infrared light: A critical evaluation. Transl Vis Sci Technol. 2025;14(6):36, https://doi.org/10.1167/tvst.14.6.36

Purpose: After cataract surgery, near-infrared (NIR) light–based optical devices are commonly used for in vivo vision quality assessment, using wavefront sensors and double-pass techniques. This study investigates the diffraction efficiencies and orders of the AT LISA tri 839MP (Carl Zeiss Meditec AG, Berlin, Germany) under visible and NIR illumination, highlighting challenges in using NIR-based devices to evaluate diffractive intraocular lenses (IOLs).

Methods: This study uses an optical bench system to generate in vitro through focus intensity data and compares the results to an optics simulation using the manufacturer's theoretically designed diffractive surface topography of the investigated trifocal IOL instead of possibly error-prone measured topography data.

Results: For visible light, through-focus curve intensities and energy efficiencies behaved as expected. However, under NIR light, near and intermediate foci showed significantly reduced intensities compared to the far focus. Energy efficiency measurements indicate suboptimal performance of the near and intermediate foci with NIR light. Under these conditions, the investigated trifocal IOL became almost monofocal.

Conclusions: The study demonstrates the wavelength-dependent behavior of the diffractive IOL, emphasizing the risks of inaccurate assessments when using NIR-based devices. It highlights the need for visible-light-based techniques for accurate evaluation and the importance of using precise surface topography data in simulations.

Translational Relevance: This research bridges the gap between basic research and clinical care by showing that vision assessments performed with NIR-light inaccurately evaluate diffractive IOLs, guiding clinicians toward visible-light techniques for accurate vision assessment.

Introduction

The implantation of multifocal intraocular lenses (MIOLs) during cataract surgery or presbyopic lens exchange is a commonly used approach to offer patients spectacle independence. The development of advanced lens designs is very complex, involving a wide range of boundary conditions. Within the group of MIOLs, diffractive multifocal IOLs (DMIOLs) use a more intricate approach than refractive MIOLs. They usually consist of a refractive base shape, serving for the far focus, with a topographical diffractive ring pattern applied on the lens surface that creates the additional focal points, as defined by their specific add power. In summary, these DMIOLs achieve their multifocality based on refraction and interference effects.[1,2] Because the human eye has its greatest sensitivity around 550 nm, as shown by the CIE photopic luminous efficiency function $V(\lambda)$,[3] DMIOLs are

generally designed for green wavelengths. This design wavelength is set at 546 nm ±10 nm in accordance with the ISO standard 11979-2:2024.[4]

For the objective analysis of the imaging properties of IOLs, optical benches, wavefront aberrometers, and double-pass systems are used. In that context, optical bench systems analyze the Airy disk, modulation transfer function (MTF), and the point spread function (PSF) of IOLs. The Airy disk is a characteristic diffraction-limited pattern of light that defines the smallest possible size to which a point light source can be imaged. The PSF describes how an imaging system would depict an ideal, punctiform object and is the corresponding intensity plot of the Airy disk but also accounts for additional aberrations in a non-diffraction limited scenario, as with the investigated DMIOL. An optical bench, as introduced in Sievers et al.,[5] uses green light, whereas others use white light (e.g., Petelczyc et al.[6]) or NIR light (e.g., Vega et al.[7,8]).

Ginis et al. developed a model eye equipped with a camera acting as the retina, where the lenses in front of the model eye enable the automated recording of a defocus curve with a series of optotypes to examine the lenses' performance requirements in visual tasks such as reading in different distances—among others for the IOL investigated here.[9]

However, when assessing the visual outcomes and imaging properties of implanted DMIOLs in a clinical context, wavefront aberrometers[10–21] and double-pass–based systems[22–28] have been used by several authors. These devices generally use light in the NIR spectral band (780–1000 nm) to determine the postoperative visual outcome and the patient's pseudophakia. The use of NIR light for in vivo assessment of vision quality has some important advantages and is based on the increasing reflectivity of the retina with increasing wavelength.[29] Furthermore, glare decreases, and the maximum permissible exposure increases,[30] are especially important for double-pass systems.

A Clarivate "Web of Science" search was used to obtain an estimated number of publications analyzing DMIOLs with devices using NIR light. This search was conducted for several commercial NIR light-using devices, which are composed in a Table (see Supplementary Table S1), yielding 12 results for wavefront aberrometers and seven for double-pass systems. For example, the search with the search parameters "iTrace AND diffractive IOL" yielded six results. However, we do not claim the reference list to be complete. A total of 396 citations related to DMIOLs and NIR light were found.

Nevertheless, DMIOLs are not optimized for NIR light, consequently leading to different visual outcomes when analyzed under these conditions. This specifically means that the results of wavefront refractive values like sphere and cylinder (lower-order aberrations), but also coma, spherical aberration and trefoil (higher-order aberrations) may be erroneous. Several recent studies are overlooking the risks of wrong assumptions when analyzing DMIOLs with NIR light, even though previous studies by Charman et al.,[31] Campbell,[32] and Vega et al.[7,8] have already shown that optical performance testing of this type of lenses is problematic.

Charman et al.[31] emphasize that wavefront aberrometers give erroneous results when analyzing pseudophakic eyes with diffractive IOLs. Gatinel[33] points out that the analysis of diffractive IOLs with double-pass systems such as the OQAS using wavelengths of 780 nm leads to an altered light distribution in the foci of the DMIOL. Thus most of the light energy is directed into the zeroth diffractive order, while much less energy ends up in the first or higher orders (i.e., in the near or intermediate focus), which are essential for the multifocality of the lens. Furthermore, Vega et al.[8] recently showed that the distribution of light energy to the focal points of a DMIOL is strongly wavelength dependent and that measurements with NIR light, instead of the design wavelength, lead to different optical performances.

Previous theoretical works about additive power and diffraction efficiency have two important implications. First, longer wavelengths like NIR light

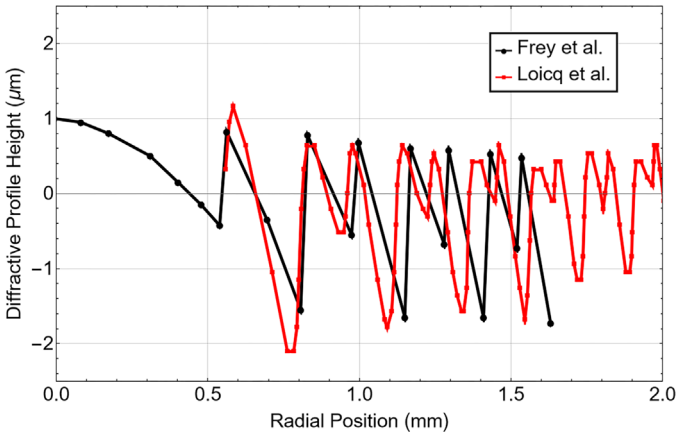

Figure 1. Comparison of two experimentally measured diffractive surface profiles of the AT LISA tri 839MP. Frey et al.[37] used a confocal microscope (MarSurf CWM 100) for the topography analysis, whereas Loicq et al.[38] used an optical profilometer (Bruker Contour GTI). Both published diffractive profiles served as a basis for further optics simulations of the investigated IOL raising the question which of the profiles is most accurate. The profiles were extracted using g3data (https://github.com/pn2200/g3data, an open-source program available under the GNU General Public License).

increase the additive power of the near and intermediate focus since diffractive power is proportionally dependent on wavelength.[34] Second, the wavefront intensity will be weaker for the near focus with respect to the far focus because diffractive efficiency decreases with longer wavelengths and more light is directed into the zeroth diffractive order.[35] As a result, the postoperative vision quality assessment of pseudophakic eyes with DMIOLs is in considerable doubt.

Recent studies derived simulation data from experimentally obtained surface topography data—for monofocal IOLs[36] and DMIOLs.[8] However, in the case of DMIOLs, discrepancies in the accuracy of these surface profiles suggest limitations in such approaches as shown in Figure 1. This study seeks to address this gap by demonstrating the wavelength and pupil size–dependent effects on through-focus curves and diffraction efficiencies of the AT LISA tri 839MP. Unlike previous research that relied on experimentally derived topography data,[37–39] we used the manufacturer's theoretically designed surface topography to achieve a more accurate optical simulation. Our results complement previous findings and further underline the need for future visible-light techniques to evaluate DMIOLs.

Methods

The experimental setup is composed of an optical bench incorporating the IOL under examination in a model eye with water immersion. The optical bench (see Fig. 2) was already published in detail by Sievers et al.[5] and is briefly explained in the following. In contrast to Sievers et al.[5], where only a green LED (λ_c = 530 nm, λ_{FWHM} = 47 nm) was used, the optical bench was equipped with three additional LEDs: a blue LED (λ_c = 463 nm, λ_{FWHM} = 23 nm), a red LED (λ_c = 628 nm, λ_{FWHM} = 15 nm) and a NIR LED (λ_c = 789 nm, λ_{FWHM} = 32 nm). The LED spectra were measured with a fiber optic spectrometer (AVASPEC-ULS4096CL-EVO; Avantes, Apeldoorn, The Netherlands).

The monochromatic LED light passes a pinhole (15 µm; Thorlabs, Newton, NJ, USA) and is collimated by an achromatic lens (f = 150 mm; AC254-150-A1, Thorlabs, Newton, New Jersey, USA). The diameter of the collimated beam is adjustable by an aperture (SM1D12C; Thorlabs). For the sake of simplicity, the model eye of the VirtIOL was used in our measurements.[40] The model eye consists of a model cornea, an off-the-shelf achromatic lens with an effective focal

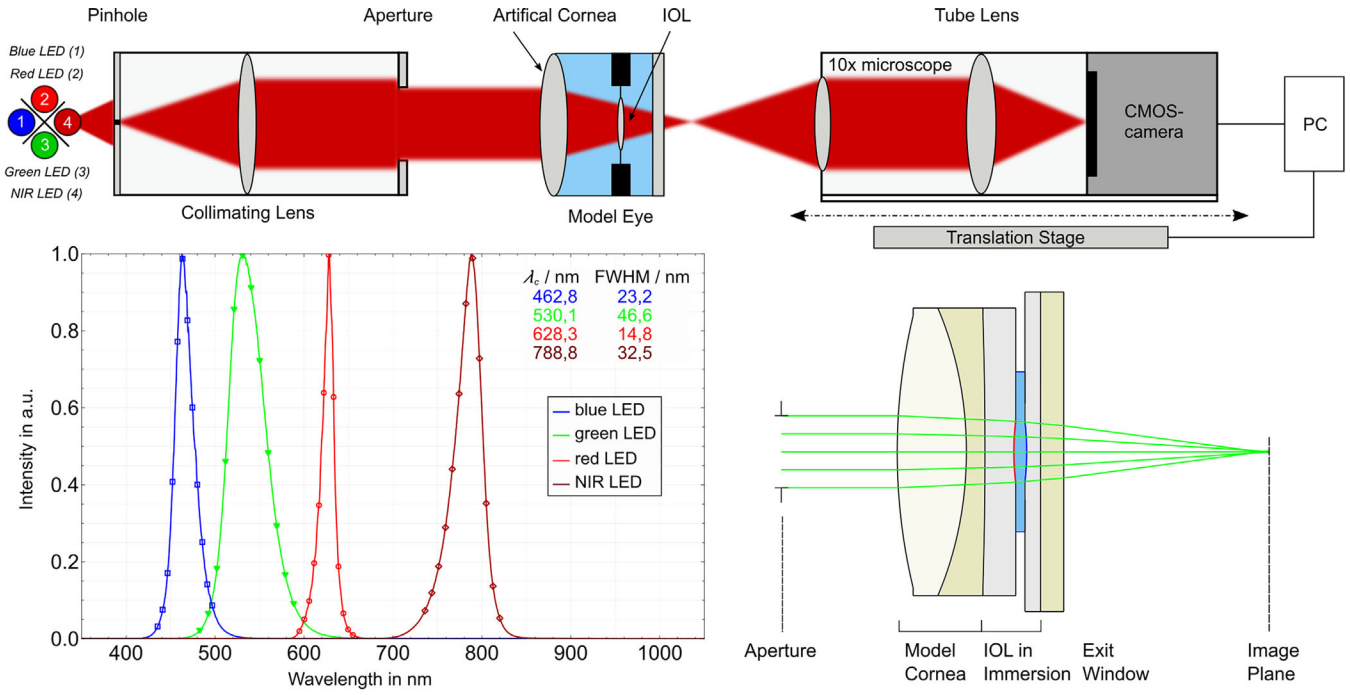

Figure 2. Schematic optical bench setup for the acquisition of three-dimensional focal light distributions. A blue (*1*), red (*2*), green (*3*), and NIR (*4*) LED were integrated into the setup. The associated spectral bands are shown at the bottom left, specified by central wavelength λ_c and FWHM (full-width half-maximum). The IOL is immersed in water within a model eye with an artificial cornea. The illuminated diameter on the IOL is adjusted with the aperture. A camera-based microscope is translated along the optical axis. The optical layout of the simulation environment is shown at the bottom right. The red IOL surface indicates a true topographical surface modeling of the diffractive IOL.

length of 40 mm and neutral spherical aberration, an IOL holder with the IOL under testing in water immersion, and a window at the back. Because the achromatic lens is in contact with water at one surface, it is no longer achromatic and free of spherical aberration and, hence, does not comply with ANSI Z80.35:2018 and ISO 11979-2:2024[4] specifications for a model eye, which should come as close as possible to the spherical and chromatic aberration of the eye. However, this study does not address the effects of polychromatic light on diffractive lenses but rather the effects of monochromatic light on diffraction efficiency and thus on the diffraction orders. The exact amount of chromatic aberration of each focus is irrelevant to the conclusions drawn in this article.

A diffractive trifocal IOL (AT LISA tri 839MP; Carl Zeiss Meditec AG, Berlin, Germany) with an optical base power of 25.00 dpt, an add power of 3.33 D for the near and 1.66 D for the intermediate focus was investigated. The illuminated area on the model cornea is adjusted using the iris diaphragm (aperture) positioned in front of the model eye. The illuminated IOL diameter d_{IOL} was determined for a set of diameters d_A of the iris diaphragm using Ansys Zemax OpticStudio (ANSYS Inc. Headquarters, Canonsburg, PA, USA). An almost linear relationship exists between the two diameters. Table 1 presents the various pupil diameters that were set during the measurement series.

Table 1. Relation Between the Aperture d_A and the Illuminated IOL Diameter d_{IOL}

d_A in mm	2.5	3.0	3.5	4.0	4.5	5.0	5.5	6.0
d_{IOL} in mm	2.12	2.54	2.96	3.38	3.80	4.22	4.65	5.07

A CMOS-camera-based microscope (microscope objective IC10 MD-Plan, NA = 0.25 [Olympus, Shinjuku, Japan] and a 150 mm achromatic tube lens) is automatically translated with an increment of s_I = 7.63 µm along the optical axis and records the two-dimensional (2D)-light distribution in the form of sequential images. The three-dimensional (3D)-light distribution of the image stack corresponds to the 3D-PSF of the IOL. The CMOS camera used in this study is a monochrome model (UI-3880CP-M-GL Rev.2; IDS Imaging Development Systems GmbH, Obersulm, Germany). According to the EMVA test report for this camera (IDS, UI-3880CP-M-GL R2, 4103099007, April 27, 2017), the linearity error in the default setting is 0.26%; hence, no linearity correction was applied. The spectral quantum efficiency of the sensor was not taken into account, as well as the intensity of the respective LEDs. This is valid because we only present normalized or relative data, except for Figure 3. Accounting for spectral quantum efficiency and optical power of the LEDs would only

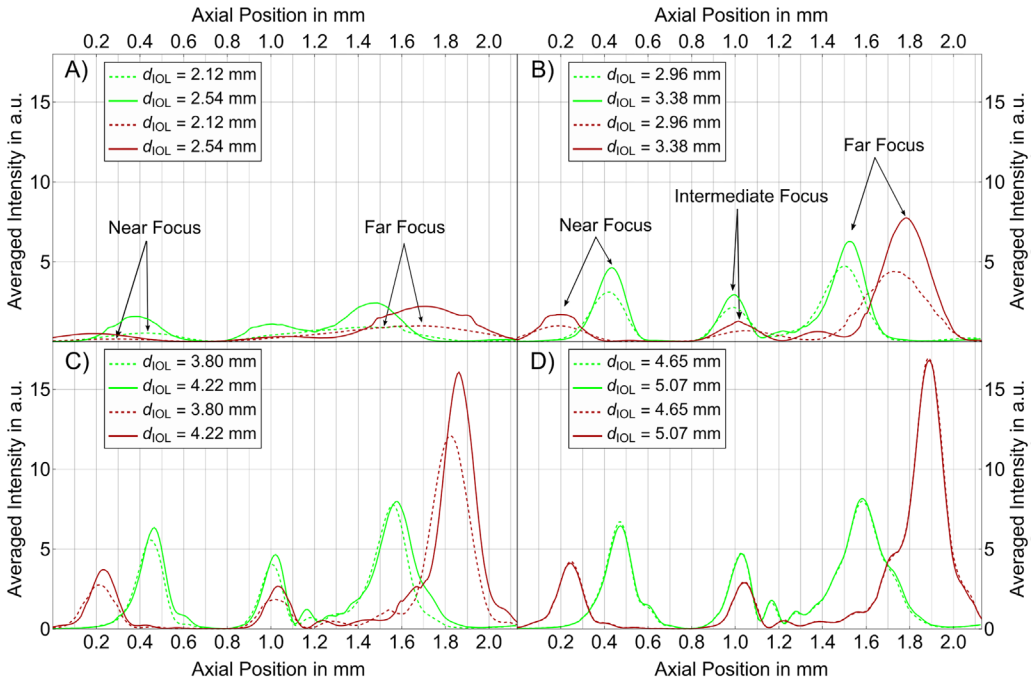

Figure 3. Overview of through-focus curves. Through-focus curves for eight different pupil diameters using a diffractive trifocal IOL (AT LISA tri 839MP; Zeiss Meditec AG) in the model eye at 530 nm illumination (green light, *green lines*) and at 789 nm Illumination (NIR light, *dark red lines*). For both wavelengths, (**A**) shows the through-focus curves for 2.12 and 2.54 mm, (**B**) for 2.96 and 3.38 mm, (**C**) for 3.80 and 4.22 mm, and (**D**) for 4.65 and 5.07 mm pupil diameters. With increasing pupil size, the intensity increases. For 2.12 mm pupil size, the IOL shows a bifocal character for green and NIR light. See text for further explanation.

lead to a scaling, but not to a deformation of the through-focus curves. In Figure 3, we present absolute values to keep the information of the pupil size dependent intensity change. However, conclusion on the spectral transmittance of the IOL must not be deduced.

Through-Focus Curve and Energy Efficiency Calculation

The captured 3D-PSF was analyzed based on a proprietary algorithm introduced by Sievers et al.[5], written in Mathematica 12.0 (Wolfram Research Europe Ltd, The Wolfram Centre, Long Hanborough, UK), to determine the through-focus curves, as well as the radial intensity distribution of rotational symmetric IOLs. We used different exposure times for the different pupil sizes and divided the intensity by the respective exposure time. This way, all curves were normalized to 1 ms and the required dynamic range of the camera for appropriately imaging in-focus and out-of-focus PSFs was reduced.

Through-focus curves show the intensity change along the optical axis. The optical axis is in the center of the images captured by the optical bench. The intensity value of each image is calculated by averaging over an area of 11 × 11 central pixels. This area was chosen to maximize the signal-to-noise ratio while maintaining the shape of the through-focus curve. Care was taken to ensure that the size of the square was small enough to avoid artifacts in the through-focus curve. Large averaging areas would smoothen the curves. The square shape was chosen over the more appropriate disc shape for easier implementation.

According to simulations, the Airy disk has a diameter of 73 µm and 60 µm for 3.5 mm and 4.5 mm aperture, respectively. This is equivalent to about 30 pixels and 25 pixels. Table 2 shows the detailed values. For a pixel size of 2.4 µm the angular size of 11 × 11 pixels corresponds to a full angle of approx. 0.5 arcmin in front of the model eye, which is half of the minimum angle of resolution. The ratio of Airy disc diameter to pinhole diameter on the camera is in the order of 3 for the apertures shown here, and thus considered as point light source.

Table 2. Relation Between Pinhole, Aperture, and Simulated Airy Disk

Aperture (mm)	Pinhole on Camera (µm)	Airy Disk on Camera (µm)
3,5	19.2	73
4,5	18.5	60

All specified values are diameters.

Before defining the fixed 11 × 11 pixel square, the entire image stack undergoes a preprocessing step to ensure the best possible alignment with the optical axis. A detailed description of the pre- and post-processing pipeline including background noise correction and centroiding is published in Sievers et al.[5]

Here, for each image another background image was recorded with the same imaging parameter, but with the beam blocked between the pinhole and the collimating lens. These background images were subtracted from the PSF images. Hence, dark current and ambient stray light were neglected.

The algorithm for determining the radial intensity distribution is based on the rotational symmetric design of IOLs, in which 3D-PSFs are rotational symmetric as well. A lateral cross-section of the 3D-PSF can consequently be transferred from a 2D to a one-dimensional (1D) light distribution, which is the radial light distribution.

Within this work, we use two efficiency terms that seem to be similar. The scalar diffraction efficiency, as common in scalar diffraction theory, treats light as a scalar wave and is described, e.g., in the theoretical work of Faklis and Morris.[35] Here, it is specified in arbitrary units and essentially corresponds to the through-focus intensity curve, representing the distribution of on axis energy. In contrast, energy efficiency η refers to the ratio of intensity within a specific focal point to the total incident intensity as described in Equation 1. Hence, contrary to the first term, the latter term also gives information on the amount of light being in the halo pattern. The energy efficiency η is theoretically defined as the ratio of light located in the focal point I_f to the total value of incident light I_L. The total intensity of an image I_{Total} is the value of I_L plus the total value of noise of the camera sensor I_{Noise} (defocused light is not considered as noise). This results in the following correlation for the energy efficiency determined with the optical bench:

$$\eta = \frac{I_f}{I_L + I_{Noise}} = \frac{I_{Airy}}{I_{Total}} \quad (1)$$

Although the in-focus 2D-PSF is known as the Airy disk and may be described by a Bessel function of the first kind, the 2D-PSF of, for example, a trifocal IOL or an out-of-focus image is not necessarily a Bessel function of the first kind. Therefore we first approximate the cross-section of the 2D-PSF by fitting a 1D-Gaussian function to the first elements of the radial intensity distribution. Next, we integrate the fitted function over 2 π to account for the total inten-

sity across the entire area, effectively simulating the rotational symmetry of the 1D-Gaussian.

Optics Simulation

An optical simulation procedure was used to verify the experimental results. It was conducted using Ansys Zemax OpticStudio 2023 R2.00 in conjunction with a user-defined surface model to accommodate true diffractive surface topographies and enhanced mathematical analysis methods to calculate the diffraction efficiencies.[34]

The simulation model comprises an in-silico representation of the artificial model eye used in the laboratory experiments. It consists of the same model cornea (achromatic doublet with an effective focal length of 40.0 mm), immersion medium (pure water), the IOL model prescription (AT LISA tri 839MP), and a glass (B270) exit window (see Fig. 2). All optical materials are modeled using dispersion formulas (Schott) covering the entire polychromatic spectral range.

The simulation was conducted using the same four polychromatic spectral bands as described in the experimental setup. The spectral intensity distribution of each spectral band was resampled into 12 weighted wavelength data points used for polychromatic simulation.

The system aperture is placed in front of the artificial model and was set to diameters of 3.5 mm and 4.5 mm (corresponds to d_{IOL} = 2.96 mm and d_{IOL} = 3.80 mm on the IOL surface) to mimic the effect of photopic and scotopic pupils on the imaging properties of the IOL, respectively. A through-focus diffraction efficiency analysis was conducted by variation of the detector distance with respect to the exit window. In the simulation, an absolute x-axis is defined, where 0 mm is at the back of the window of the model eye. The measurement data only has a relative x-axis. In order to present both data side by side, the relative x-axis was shifted so that the far focus overlaps in green at d_{IOL} = 2.96 mm (Fig. 4).

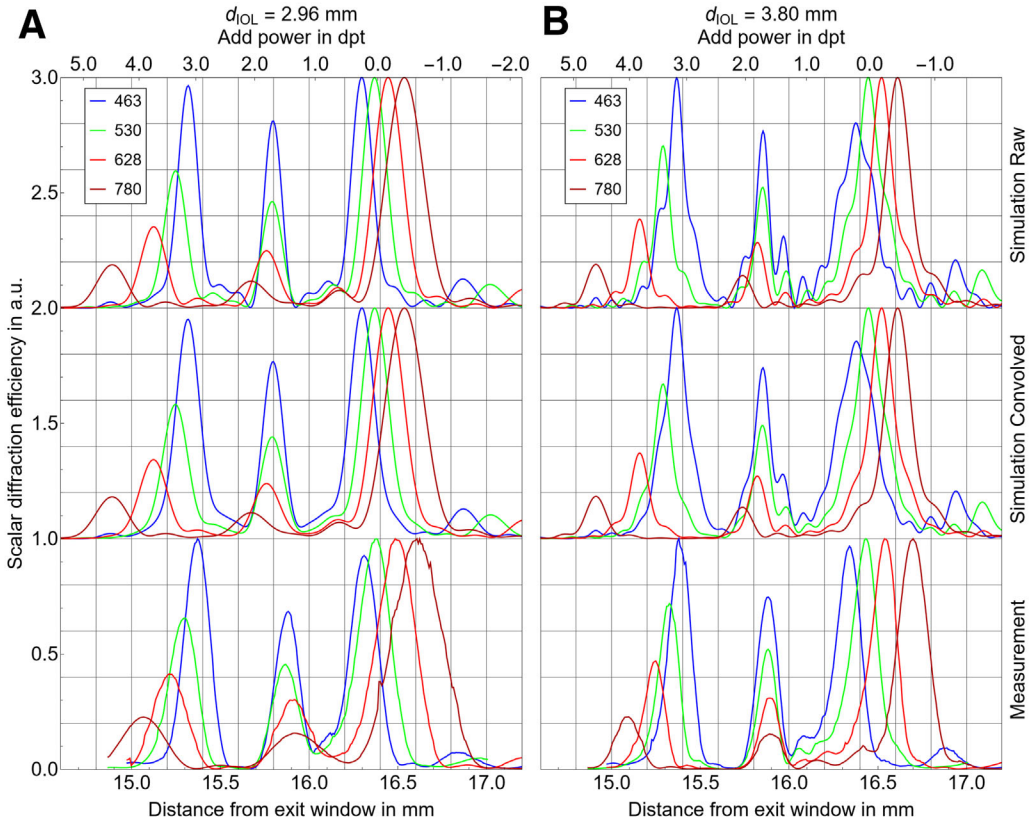

Figure 4. Focal wavelength dependency. Overview of through-focus curves using a diffractive trifocal IOL (AT LISA tri 839MP; Zeiss Meditec AG) and two different pupil diameters: (**A**) 2.96 mm and (**B**) 3.80 mm. All curves were normalized. For the sake of clarity, the through-focus curves of the simulation were shifted by +2 a.u. (*top*). For a better agreement with the measurement data (*bottom*), the simulation curves were convolved with a Gaussian filter width of 84 µm (for A) and 50 µm (for B) and shifted by +1.0 a.u. (*middle*). The bottom axis is presented in mm. A secondary axis in the top is presented in diopters (dpt). The position of 0 dpt was defined by the theoretical far focus position at 546 nm wavelength.

Results

The through-focus curves for the investigated IOL under green light (shown in green) and NIR light (shown in dark red) for various pupil sizes ranging from 2.12 mm to 5.07 mm are shown in Figure 3. In each diagram, two pupil sizes are compared (dashed lines represent the smaller and solid lines the larger d_{IOL}). Using green light, the through-focus intensity for $d_{IOL} \approx 2.1$ mm (top left diagram, dashed green line) reveals two axially extended intensity distributions. Hence, the IOL appears to be bifocal with EDOF characteristics (see Fig. 3A and Supplementary Table S2). By increasing d_{IOL} to about 2.5 mm (solid line), the through-focus curve already shows trifocal behavior. Under NIR light, both through-focus curves are strongly smeared out, resulting in an undefined mixture of bifocal and EDOF IOL. On the top right, in Figure 3B, three distinct foci of similar intensity are visible at both wavelengths. Increasing d_{IOL} further, as depicted in Figures 3C and 3D, the near and far foci shift to greater axial positions. In contrast, the intermediate foci are almost pupil size-independent (cf. Fig. 3 and Supplementary Table S2).

With increasing pupil size, the greatest shift in axial position is exhibited by the far focus under NIR light illumination ($\Delta = 0.18$ mm), followed by the far focus under green light ($\Delta = 0.12$ mm) illumination. Looking at the distance D between the near and far focus ($D_{NEAR\text{-}FAR}$), there is no remarkable change for green light over the pupil size ($D_{NEAR\text{-}FAR} \approx 1.10$ mm), whereas under NIR light an increase of $\Delta D_{NEAR\text{-}FAR} = 0.12$mm could be seen between $d_{IOL} \approx 2.9$ mm ($D_{NEAR\text{-}FAR} \approx 1.52$ mm) and $d_{IOL} \approx 5.9$ mm ($D_{NEAR\text{-}FAR} \approx 1.64$ mm). This implies that the pupil size dependence for green light is rather small but greater for NIR light. Switching from green to NIR light, the distance between near and far focus increases from $D_{NEAR\text{-}FAR} \approx 1.10$ mm to $D_{NEAR\text{-}FAR} \approx 1.64$ mm. At the same time, the near focus shifts to smaller axial positions for NIR light compared to green light.

Briefly, with increasing pupil size, near and far foci shift to greater axial positions - except for 2.12 mm pupil size, where the IOL shows an overlap of a smeared near and intermediate focus leading to a bifocal character for green and NIR light, which then turns into a trifocal character with a shift of the near focus to smaller axial positions.

The optics simulation could confirm the results obtained for green and NIR light. Figure 4 compares these simulation results with the experimental data. The top row shows the simulation data, whereas the bottom row presents the measurement data. Results for the smaller pupil size (3.5 mm $\approx d_{IOL}$ of 2.96 mm) are shown on the left, and for the larger one (4.5 mm $\approx d_{IOL}$ of 3.80 mm) on the right. Note that in this representation, all curves are intensity normalized. Since the optical simulation could not yet provide complete agreement with the measurement data and the microscope's depth of field also has to be taken into account, the simulation curves shown here were convolved with a Gaussian filter width of 84 µm (Fig. 4A) and 50 µm (Fig. 4B) to account for the respective depth-of-fields due to the effective numerical apertures (NA). The objective lens and its nominal NA do not primarily determine the depth of field, but rather the light cone emerging from the model eye. This cone effectively reduces the used NA of the objective, because the back aperture is not fully illuminated. Consequently, the objective's full NA is not exploited because of the narrower illumination cone from the model eye.

The measurement data and the convolved simulation are in quite good agreement, considering, for example, the small number of averaged pixels. With larger pupil sizes, the IOL is trifocal for all tested wavelengths. Here, with increasing wavelength, the distance between the near and far focus ($D_{NEAR\text{-}FAR}$) grows, too, resulting in greater axial shifts to smaller positions for the near and greater positions for the far focus.

However, the intensities of near (I_{near}), intermediate (I_{int}), and far focus (I_{far}), as their intensity ratios, change with wavelength. In contrast to visible light, the intensity ratio of the near or intermediate focus to the far focus decreases for NIR light. The intensity ratio of the peaks decreases with increasing wavelengths since more light falls into the far focus (see Fig. 3). The simulation data shows that with increasing wavelength, the intensity of the near and intermediate focus decreases relative to the far focus. Supplementary Table S3 shows the intensity ratios of the near to far focus (I_{near}/I_{far}) and intermediate to far focus (I_{int}/I_{far}) for all four wavelengths, comparing simulated data (S) and measurement data (M). There is a decreasing tendency in the intensity ratio values for near and intermediate focus with increasing wavelength, i.e., the far focus is more dominant than the other foci. This tendency is also depicted in Figure 5. From blue to NIR light, the ratio falls to approximately one-quarter.

This behavior is even more striking when looking at energy efficiencies. As defined above, energy efficiency measures the amount of light contributing to the individual foci. Figure 6 presents a comparable overview of each focus's pupil size-dependent energy efficiency η using green (left) and NIR light (right) to

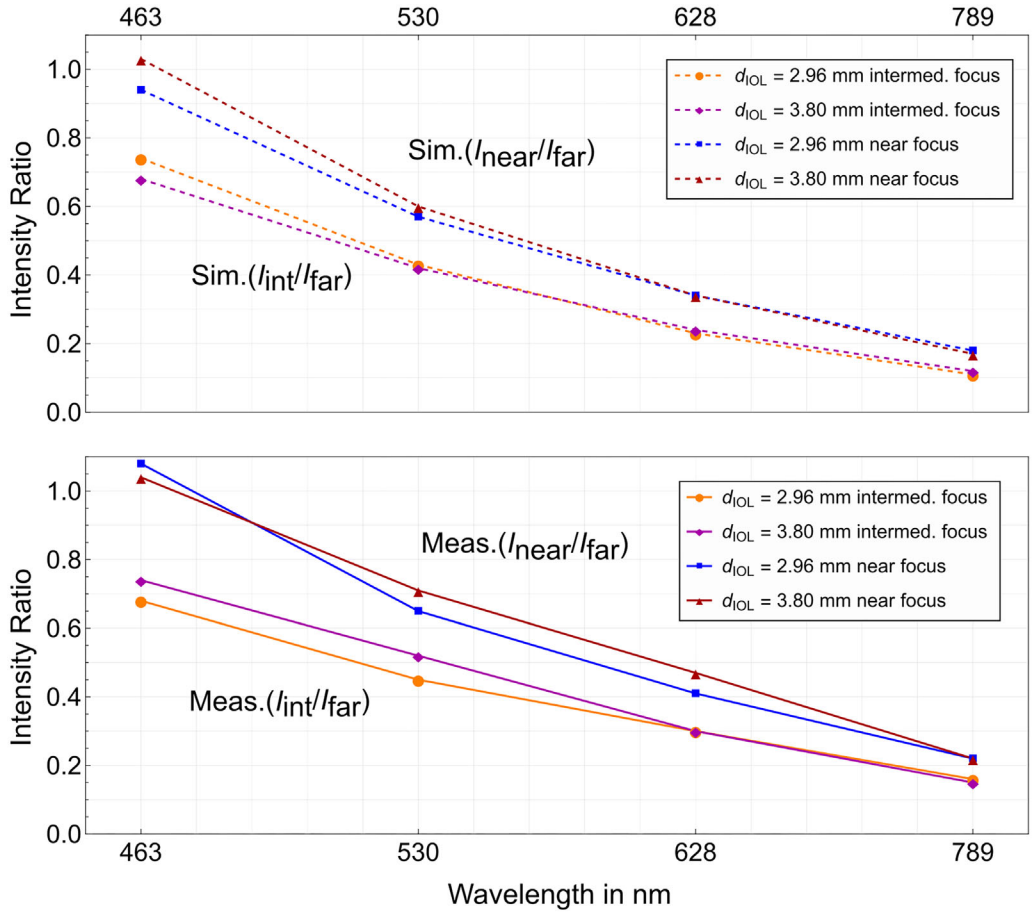

Figure 5. Wavelength dependence of intensity ratios. The figure shows the intensity ratios for the near and far focus (I_{near}/I_{far}) as for the intermediate and far focus (I_{int}/I_{far}) for all four wavelengths, comparing simulated data (*top*: Sim., *dashed lines*) and measurement data (*bottom*: Meas., *solid lines*). A decreasing tendency in the intensity ratio values for near and intermediate focus is found with increasing wavelength.

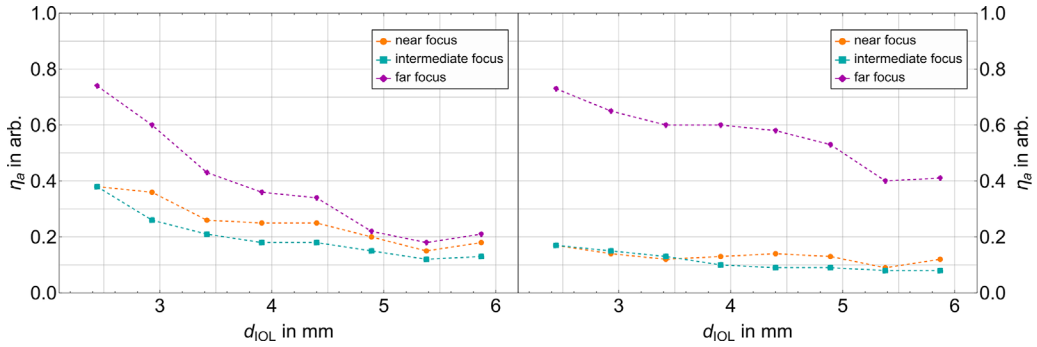

Figure 6. Calculated energy efficiencies from measurement data. Overview of the pupil size-dependent energy efficiencies of a diffractive trifocal IOL (AT LISA tri 839MP; Zeiss Meditec AG) for the near (*yellow circle*), intermediate (*light blue square*), and far focus (*purple diamond*). *Left*: 530 nm illumination (green light). *Right*: 789 nm illumination (NIR light). Using NIR light, much more energy is diffracted into the far focus and less light into the near and intermediate focus compared to green light, resulting in a monofocal behavior of the trifocal IOL under NIR light.

highlight the difference between design wavelength and NIR-based analysis. For both wavelengths, the energy efficiency of each focus decreases with increasing pupil size because of a loss of light in halos and higher-order aberrations.

Although the far focus efficiency for green light and small pupil sizes is almost twice as high compared to the other foci, it approaches the other foci's energy efficiencies at large pupil sizes. However, using NIR light, the far focus is more than four times as efficient

as the other foci and remains at approximately four times higher efficiencies for larger pupil sizes. While comparing both wavelengths, the near and intermediate foci energy efficiencies decrease from about 25% (near) and 18% (intermediate) for green light to about 14% (near) and 9% (intermediate) for NIR light at 4.5 pupil diameter. These measurement findings are consistent with our simulation findings. Hence, in using NIR light, much more energy is diffracted into the far focus and less into the near and intermediate focus compared to green light. This implies that although this specific diffractive IOL is trifocal for visible light, it becomes almost monofocal for NIR light.

Discussion

Regardless of the numerous publications addressing the challenge of evaluating the optical performance of DMIOLs under NIR light, a significant amount of recent research (see Supplementary Table S1) still neglects the findings presented in these studies. To get a subjective impression of the imaging properties of a DMIOL before implantation, optical see-through devices like, for example, the VirtIOL (10Lens S. L. U., Terrassa, Spain), which imprint the optical properties of the IOL onto the patient's retina, were developed and can be used for in vivo studies. Newer systems used for IOL vision simulation are, for example, the ACMIT IOL simulator (Austrian Center for Medical Innovation and Technology, Vienna, Austria)[41] and the RALV system (Real Artificial Lens Vision, FirstQ, Mannheim, Germany). Other systems like the VAO simulator (VOPTICA, Murcia, Spain) or SimVis Gekko (2EyesVision, Madrid, Spain) are based on adaptive optics technology, which dynamically modify optical wavefronts to simulate different optical corrections, including IOLs, spectacles, and contact lenses. Letter uses a tunable lens system to replicate different lens designs without requiring physical lens replacement.

However, to objectively assess the optical performance of DMIOLs and confirm optical simulations, in vitro studies are performed on optical benches. These are either commercially available or specifically designed optical benches. The general characteristics of currently used benches are a collimated light beam, an IOL installed in a model eye, a camera for recording the 2D-PSF, and hardware for image data processing. To ensure the comparability of optical IOL properties, the updated ISO standard 11979-2:2024[4] was introduced in 2024, which defines specific technical conditions for experimental IOL analysis on optical benches.

A commercial optical bench is the OptiSpheric IOL PRO2 (Trioptics GmbH, Wedel, Germany), which was used, for example, by Borkenstein et al., for MTF analysis of several IOL designs.[42] Ravalico et al. were among the first to use a specifically designed optical bench to calculate energy efficiencies of IOLs from 2D-PSF images.[43] Several authors currently use optical benches for MTF or through-focus intensity analysis of different IOLs.[44–48]

The ANSI Z80.35:2018 (Unpublished data, 2014) and ISO 11979-2:2024[4] define specifications for a model eye. Based on these specifications, a polychromatic analysis of the IOL is then carried out to generate a polychromatic MTF, which in turn is used to predict visual acuity. However, absolute longitudinal chromatic aberrations, as they might be influenced by an inappropriate model cornea, are not relevant here as we do not predict the polychromatic visual acuity. Generally, a phase profile of the diffraction surface of the IOL is sufficient to describe these influences discussed here.

Monofocal IOLs use the principle of refraction to correct vision for a single distance. Refractive multifocal IOLs incorporate different zones of varying optical power to create multiple foci. For refractive IOLs, these NIR-light-using systems presumably do not pose a problem in determining optical properties since the PSF and, thus the Airy disk of refractive lenses scale with wavelength. Hence, this allows the optical properties at wavelengths in the NIR spectrum to be recalculated for green light, for which IOLs are generally designed. At great distances and using small-angle approximation, the angle θ between non-diffracted light and the first intensity minimum of the diffracted light is given by:

$$\theta \approx 1.22\frac{\lambda}{d} \tag{2}$$

Here, λ is the wavelength, and d is the aperture diameter. This approach is valid for refractive lenses but not DMIOLs. They usually consist of a refractive base shape, serving for the far focus, with a topographical diffractive ring pattern applied on the lens surface that creates additional focal points. These additional foci are based on constructive interference due to the specific step heights of the ring pattern, inducing appropriate phase shifts. Often, the step heights are calculated for green light.

In this context, longitudinal chromatic aberration (LCA) manifests in two different ways. First, in a nonlinear wavelength dependence of the focal length based on the refractive nature of the far focus, and second, in the case of DMIOLs, in a linear wavelength dependence of near and intermediate foci due to the diffractive nature of these foci. Because

near and intermediate focus are based on the nonlinearly wavelength dependent refractive base power and linearly wavelength dependent diffractive add power, the total refractive power arises from the linearly and nonlinearly wavelength dependent effects.

The pupil-dependent foci presumably shift due to spherical aberration and the illumination of different optical zones of the IOL. Wavelength-dependent shifts of the far focus result from the lens material's inherent chromatic properties and the amount of chromatic aberration induced by the model cornea. The same holds true for the near and intermediate foci with an additional axial shift due to the superposition with the diffractive chromatic aberration of the respective add powers. For the intermediate focus we observed almost no pupil size dependent shift when comparing both pupil sizes in Figure 4 or the shift over eight pupil sizes in in Figure 3 and only a minimal wavelength dependent shift of approximately 0.1 mm in Figure 4. It seems that the intermediate focus shift is only minimally influenced by the wavelength for the measurement data since the diffractive proportion of the LCA and the refractive proportion of the LCA are apparently similar and cancel each other out. The near focus experiences an axial shift to smaller values because of the diffractive LCA of the respective add powers.

The imaging performance of DMIOLs depends on the wavelength in multiple ways. Fiala et al.[34] and Faklis et al.[35] provide a detailed analytical description of the diffractive working principles. The key concepts of these theoretical studies are explained in the following. First, the add-power increases linearly with wavelength. The zeroth diffraction order is used for distance vision and is not affected by diffractive chromatic dispersion effects. This applies for the investigated DMIOL with its far focus produced by the refractive base lens and the zeroth orders of the two diffractive profiles. The analysis demonstrates that the add-power(s) of diffractive multifocal lenses is linearly dependent on the ratio of $\lambda_F/\ \lambda_0$, where λ_F is the analysis wavelength and λ_0 the design wavelength of the IOL. Any measurement of add powers and associated defocus curves must consider the wavelength-dependent scaling of the diffractive add-power. Erroneous measurement may result if this is done improperly. Because the near and intermediate focus of the investigated DMIOL are produced by the 1st order of the 2nd diffraction profile and the first order of the 1st diffraction profile,[38] respectively. The longer the wavelength, the greater the distance between the additional and the far focus due to the add-power dependent focus shift (see Figs. 3 and 4). Furthermore, the wavelength-dependent focal shift scales with the add power. This is observed by the stronger dependence of the near focus compared to the intermediate focus. However, the exact position of the single foci itself is irrelevant here and may be influenced by the model cornea.

A second important aspect is the wavelength dependence of diffraction efficiency. It defines the proportion of incoming light at a given wavelength is distributed in a particular diffraction order and its associated add-power. Measurement data and simulation of the used DMIOL show that with increasing wavelength, more light is distributed into the far focus (see Figs. 4 and 5). Multifocal IOL designs use at least two significantly effective diffraction orders to create bifocal optics or three significantly effective diffraction orders to create trifocal IOLs. Four or more diffraction orders can be used to create quadrifocal or even higher-focal optical designs. The AcrySof IQ PanOptix IOL (Alcon, Geneva, Switzerland), for example, uses a quadrifocal approach.[49] The used diffraction orders for vision are typically, but not necessarily, neighboring diffraction orders. As stated before, the design of DMIOLs is generally conducted at a design wavelength λ_0.

A metric for the performance analysis of DMIOLs is the energy efficiency mentioned above, as it considers scattering, aberration, and out-of-focus images for each focus. In 2023, Vega et al.[8] analyzed the same diffractive trifocal IOL among others, employing the so called "light-in-the-bucket metric" to calculate energy efficiencies. In contrast, our method uses a Gaussian fitting function and additionally presents through-focus curves. Notably, the relationship between energy efficiencies ratios derived from experimental and simulation data is consistent across both setups but the magnitudes differ. Table 3 comprises the findings of Vega et al.[8] and our study on the AT LISA tri 839MP and compares the measured and simulated energy efficiencies of near, intermediate, and far focus, as well as the ratios of the near-to-far and intermediate-to-far focus energy efficiency. For instance, our approach assigns more energy to the near focus than the far focus compared to the measurements of Vega et al.,[8] likely because of the differing methods used to determine energy efficiencies. Notably, the sum of the foci's energy efficiencies never reaches 100% because of a loss of energy caused by halos, aberrations, and light scattering. The definition of energy efficiency is not standardized, and several approaches exist to define it. The energy efficiency values vary between our measurement and simulation. Although the experimental values were determined by the above-described Gaussian method, the simulated efficiency is the squared total of the electric field amplitudes in the respective image distance after calculating the

Table 3. Energy Efficiencies of AT LISA tri 839 MP for Each Focus at IOL Pupil 4.5 Mm Compared Between Vega et al.[8] and Our Results

	Near Focus		Intermediate Focus		Far Focus	
	Visible	NIR	Visible	NIR	Visible	NIR
Measurement						
Vega et al.[8]	0.27	0.16	0.18	0.08	0.47	0.75
Ratio	57%	21%	38%	10%		
This paper	0.25	0.14	0.18	0.09	0.34	0.58
Ratio	73%	24%	52%	15%		
Simulation						
Vega et al.[8]	0.25	0.11	0.15	0.07	0.43	0.61
Ratio	58%	18%	34%	11%		
This paper	0.15	0.1	0.11	0.07	0.21	0.52
Ratio	71%	19%	52%	14%		

The ratios are defined as near-to-far focus and intermediate-to-far focus energy efficiency for each wavelength. Visible corresponds to $\lambda_c = 530$ nm, NIR corresponds to $\lambda_c = 780$ nm.

diffraction integral according to Fiala et al.[34] However, because optical power or photometric quantities are not included in the simulation, the absolute values are arbitrarily scaled. Therefore we compare the experimentally determined efficiency ratios of the different foci with the simulated ones finding a good agreement. Whereas Vega et al.[8] used topographical data of the IOL surface measured with confocal microscopy to simulate the IOL performance[8], we use the manufacturer's genuinely designed diffractive surface topographies for the optics simulation and the formulas from Fiala et al.[34]

Furthermore, our study reports different near focus add powers compared to the findings in Vega et al.,[8] who used the same wavelengths and pupil sizes in their study. We observed 5.03 dpt for NIR light and 3.4 dpt for green light, compared to 4.8 dpt and 3.3 dpt, respectively. This discrepancy may be attributed to the difference in base power of the investigated trifocal IOL, the deviation of the illuminated IOL diameter (consequently variable illuminated optical zones) and different diffractive surface profiles.

To estimate the wavelength-dependent focal positions 546 nm, as defined by the ISO standard 11979-2:2024, we used a cubic function to fit the axial focus positions to the wavelength. Especially for small wavelength ranges, we found an almost linear dependence. Exemplary for pupil of 4.5 mm ($d_{IOL} = 3.80$ mm), the far, near and intermediate foci were shifted by 14 µm, −3 µm and −19 µm, respectively. Our measurement data shows a broadening of the near, intermediate, and far focus for each pupil size with increasing wavelength. The simulation data does not show that behavior. Further, the intermediate focus, which shifts to smaller axial positions in the simulation, shifts to greater positions in the experiment (see Fig. 4). This may have different mutually complementary reasons (e.g., decentration or imprecise determined distances of the model eye). Although the far focus appears similar for all wavelengths at the small pupil size, the far focus with blue light is wider in the simulation compared to the experiment with the larger pupil size. Nevertheless, the wavelength dependence of the diffraction efficiency and diffractive orders of the investigated DMIOL is observable for both—simulation and measurement.

Our demonstration that a diffractive trifocal IOL can become almost monofocal using NIR light highlights the potential source of error and risk when using such wavelengths as integrated in devices designed to determine the vision quality. Hence, caution is required to conclude visual assessment obtained by NIR-based methods—the results of lower- and higher-order aberrations are likely to be wrong. Our findings agree with previously established theoretical works on diffractive power and diffraction efficiency and show that the diffraction orders of a diffractive IOL are particularly shifted under NIR light.[34,35] Therefore an optical performance assessment with NIR light will lead to erroneous assumptions of the DMIOLs near or intermediate-focus performance and may lead to misleading recommendations for the implantation of DMIOLs. Hence, visible light, preferably green light (around 520-570 nm), must be used. Low-intensity levels within this spectrum are recommended to minimizing glare and discomfort. However,

the low retinal reflectance may be challenging for the light detection.

To the best of our knowledge, measuring diffractive optics with wavefront sensors poses a general challenge. This is because multiple wavefronts, including those from higher diffraction orders, converge on the microlenses of the wavefront sensor, generating numerous points. Consequently, it becomes difficult to unambiguously associate these points with the correct focal point.

The key distinction of our study compared to previous research using experimentally obtained topography data for their simulation is that we used the manufacturer's theoretically designed surface topography data of the AT LISA tri 839MP. This allowed us to achieve the most accurate optical simulation data for this commonly implanted DMIOL and to provide further evidence of focal wavelength dependence by analyzing four different wavelengths. Please note that the exact change in energy efficiency depends on the exact lens design. Hence, not all statements can be generalized for every diffractive IOL. Keep in mind that diffractive IOLs may only be examined with visible light, for which they were developed. In particular, postoperative assessment of the quality of vision of DMIOLs under NIR light must inevitably produce incorrect results. In this case, conclusions on the in vivo imaging performance of DMIOLs in publications that have already been published cannot be considered reliable.

Acknowledgments

Supported by DFG grant number 469107515.

Presented at the Deutsche Ophthalmologische Gesellschaft (DOG) conference, Berlin, Germany, September 29 to October 2, 2022.

Disclosure: **R. Elsner**, None; **M. Gerlach**, Carl Zeiss Meditec AG (E); **S. Bohn**, None; **J. Sievers**, None; **H. Stolz**, None; **R.F. Guthoff**, None; **O. Stachs**, None; **K. Sperlich**, None

References

1. Davison JA, Simpson MJ. History and development of the apodized diffractive intraocular lens. *J Cataract Refract Surg*. 2006;32:849–858.
2. Alió JL, Pikkel J, eds. *Multifocal Intraocular Lenses: The Art and the Practice*. Berlin: Springer International Publishing; 2019.
3. I. O. for Standardization. ISO/CIE 23539:2023 | CIE TC 2-93 - Photometry—The CIE system of physical photometry. Available at: https://www.iso.org/obp/ui/#iso:std:iso-cie:23539:ed-1:v1:en:ref:4:~:text=This%20document%20was%20prepared%20by,CIE%20170%2D2:2015. Accessed April 16, 2025.
4. I. O. for Standardization. I. O. for Standardization, ISO 11979-2:2024. *ISO*. Available at: https://www.iso.org/standard/55682.html. Accessed April 16, 2025.
5. Sievers J, Elsner R, Bohn S, et al. Method for the generation and visualization of cross-sectional images of three-dimensional point spread functions for rotationally symmetric intraocular lenses. *Biomed Opt Express*. 2022;13:1087–1101.
6. Petelczyc K, Kolodziejczyk A, Błocki N, et al. Model of the light sword intraocular lens: in-vitro comparative studies. *Biomed Opt Express*. 2020;11:40–54.
7. Vega F, Millán MS, Vila-Terricabras N, Alba-Bueno F. Visible versus near-infrared optical performance of diffractive multifocal intraocular lenses. *Invest Ophthalmol Vis Sci*. 2015;56:7345–7351.
8. Vega F, Faria-Ribeiro M, Armengol J, Millán MS. Pitfalls of using NIR-based clinical instruments to test eyes implanted with diffractive intraocular lenses. *Diagnostics*. 2023;13:1259.
9. Ginis HS, Tsoukalas S, Christaras D, Artal P. Visually relevant on-bench through-focus analysis of intraocular lenses. *Biomed Opt Express*. 2024;15:7056.
10. Jun I, Choi YJ, Kim EK, Seo KY, Kim T. Internal spherical aberration by ray tracing-type aberrometry in multifocal pseudophakic eyes. *Eye*. 2012;26:1243–1248.
11. Santhiago M, Netto M, Barreto J, Gomes B, Schaefer A, Kara-Junior N. Wavefront analysis and modulation transfer function of three multifocal intraocular lenses. *Indian J Ophthalmol*. 2010;58:109–113.
12. Pilger D, Homburg D, Brockmann T, Torun N, Bertelmann E, Von Sonnleithner C. Clinical outcome and higher order aberrations after bilateral implantation of an extended depth of focus intraocular lens. *Eur J Ophthalmol*. 2018;28:425–432.
13. Seo JG, Choi MJ, Seo KY, Kim EK, Kim TI. Clinical outcomes of patients fitted with bifocal and trifocal diffractive intraocular Lenses. *J Korean Ophthalmol Soc*. 2018;59:325–331.
14. Haddad JS, Gouvea L, Ferreira JL, Ambrósio R, Waring GO, Rocha KM. Impact of a chromatic

aberration-correcting intraocular lens on automated refraction. *J Refract Surg*. 2020;36:334–339.
15. Ju RH, Wu ZM, Aier Eye Hospital, Jinan University, Guangzhou 510071, Guangdong Province, China, *et al.* Comparison of visual performance with iTrace analyzer following femtosecond laser-assisted cataract surgery with bilateral implantation of two different trifocal intraocular lenses. *Int J Ophthalmol*. 2023;16:1773–1781.
16. Mojzis P, Kukuckova L, Majerova K, Liehneova K, Piñero DP. Comparative analysis of the visual performance after cataract surgery with implantation of a bifocal or trifocal diffractive IOL. *J Refract Surg*. 2014;30:666–672.
17. Velasco-Barona C, Corredor-Ortega C, Mendez-Leon A, et al. Influence of angle κ and higher-order aberrations on visual quality employing two diffractive trifocal IOLs. *J Ophthalmol*. 2019;2019(1):7018937.
18. Garzón N, García-Montero M, López-Artero E, Poyales F, Albarrán-Diego C. Influence of trifocal intraocular lenses on standard autorefraction and aberrometer-based autorefraction. *J Cataract Refract Surg*. 2019;45:1265–1274.
19. García-Bella J, Ventura-Abreu N, Morales-Fernández L, et al. Visual outcomes after progressive apodized diffractive intraocular lens implantation. *Eur J Ophthalmol*. 2018;28:282–286.
20. Carballo-Alvarez J, Vazquez-Molini JM, Sanz-Fernandez JC, et al. Visual outcomes after bilateral trifocal diffractive intraocular lens implantation. *BMC Ophthalmol*. 2015;15:26.
21. Alió JL, Plaza-Puche AB, Alió Del Barrio JL, et al. Clinical outcomes with a diffractive trifocal intraocular lens. *Eur J Ophthalmol*. 2018;28:419–424.
22. Moreno LJ, Piñero DP, Alió JL, Fimia A, Plaza AB. Double-pass system analysis of the visual outcomes and optical performance of an apodized diffractive multifocal intraocular lens. *J Cataract Refract Surg*. 2010;36:2048–2055.
23. Lee YW, Choi CY, Moon K, et al. Clinical outcomes of new multifocal intraocular lenses with hydroxyethyl methacrylate and comparative results of contrast sensitivity, objective scatter, and subjective photic phenomena. *BMC Ophthalmol*. 2022;22:379.
24. Liao X, Lin J, Tian J, Wen B, Tan Q, Lan C. Evaluation of optical quality: ocular scattering and aberrations in eyes implanted with diffractive multifocal or monofocal intraocular lenses. *Curr Eye Res*. 2018;43:696–701.
25. Chen T, Yu F, Lin H, et al. Objective and subjective visual quality after implantation of all optic zone diffractive multifocal intraocular lenses: a prospective, case-control observational study. *Br J Ophthalmol*. 2016;100:1530–1535.
26. Hwang H, Shin HY, Joo C-K. Double-pass system (Optical Quality Analysis System) for analysis of the multifocal function of a diffractive multifocal intraocular lens (Acrysof ReSTOR) compared to a monofocal intraocular lens (Acrysof IQ). *J Opt Soc Korea*. 2014;18:110–117.
27. Castillo-Gómez A, Carmona-González D, Martínez-de-la-Casa JM, Palomino-Bautista C, García-Feijoo J. Evaluation of image quality after implantation of 2 diffractive multifocal intraocular lens models. *J Cataract Refract Surg*. 2009;35:1244–1250.
28. Fernández J, Burguera N, Rocha-de-Lossada C, Rachwani-Anil R, Rodríguez-Vallejo M. Influence of a multifocal intraocular lens centration and eye angles on light distortion and ocular scatter index. *Graefes Arch Clin Exp Ophthalmol*. 2023;261:2291–2299.
29. Van Norren D, Tiemeijer LF. Spectral reflectance of the human eye. *Vis Res*. 1986;26:313–320.
30. International Commission on Non-Ionizing Radiation Protection. Revision of guidelines on limits of exposure to laser radiation of wavelengths between 400 nm and 1.4 microm. *Health Phys*. 2000;79:431–440.
31. Charman WN, Montes-Mico R, Radhakrishnan H, Papadopoulos R, Bachariou A. Can we measure wave aberration in patients with diffractive IOLs? *J Cataract Refract Surg*. 2007;33:1997.
32. Campbell CE. Wavefront measurements of diffractive and refractive multifocal intraocular lenses in an artificial eye. *J Refract Surg*. 2008;24:308–311.
33. Gatinel D. Double pass–technique limitations for evaluation of optical performance after diffractive IOL implantation. *J Cataract Refract Surg*. 2011;37:621–622.
34. Fiala W, Pingitzer J. Analytical approach to diffractive multifocal lenses. *Eur Phys J Appl Phys*. 2000;9:227–234.
35. Faklis D, Morris GM. Spectral properties of multiorder diffractive lenses. *Appl Opt*. 1995;34:2462.
36. Barbero S, Marcos S, Montejo J, Dorronsoro C. Design of isoplanatic aspheric monofocal intraocular lenses. *Opt Express*. 2011;19:6215.
37. Frey K, Hage H, Gerlach M, Brunner R. Topography Profiling: Measuring the topography of soft ophthalmological components immersed in water. *Opt Photon*. 2015;10(5):27–30.
38. Loicq J, Willet N, Gatinel D. Topography and longitudinal chromatic aberration characterizations of refractive–diffractive multifocal intraocu-

lar lenses. *J Cataract Refract Surg*. 2019;45:1650–1659.
39. Mendroch D, Altmeyer S, Oberheide U. Characterization of diffractive bifocal intraocular lenses. *Sci Rep*. 2023;13:908.
40. Gerlach M, Guthoff R, Stachs O, Bohn S, Sperlich K. Präklinische Bewertung von Intraokularlinsen durch simulierte Implantation. *Klin Monatsbl Augenheilkd*. 2018;235:1332–1341.
41. Brezna W, Lux K, Dragostinoff N, et al. Psychophysical vision simulation of diffractive bifocal and trifocal intraocular lenses. *Trans Vis Sci Tech*. 2016;5(5):13.
42. Borkenstein AF, Borkenstein EM, Luedtke H, Schmid R. Impact of decentration and tilt on spherical, aberration correcting and specific aspherical intraocular lenses; an optical bench analysis. *Ophthalmic Res*. 2022;65:425–436.
43. Ravalico G, Parentin F, Sirotti P, Baccara F. Analysis of light energy distribution by multifocal intraocular lenses through an experimental optical model. *J Cataract Refract Surg*. 1998;24:647–652.
44. Peli E, Lang A. Appearance of images through a multifocal intraocular lens. *J Opt Soc Am A*. 2001;18:302–309.
45. Castignoles F, Flury M, Lepine T. Comparison of the efficiency, MTF and chromatic properties of four diffractive bifocal intraocular lens designs. *Opt Express*. 2010;18:5245–5256.
46. Hill W, Carson D, Hong X, Karakelle M. Optical bench performance of AcrySof IQ ReSTOR, AT LISA tri, and FineVision intraocular lenses. *Clin Ophthalmol*. 2014:8:2105–2113.
47. Kawamorita T, Uozato H. Modulation transfer function and pupil size in multifocal and monofocal intraocular lenses in vitro. *J Cataract Refract Surg*. 2005;31:2379–2385.
48. Lee S, Choi M, Xu Z, Zhao Z, Alexander E, Liu Y. Optical bench performance of a novel trifocal intraocular lens compared with a multifocal intraocular lens. *Clin Ophthalmol*. 2016;10:1031–1038.
49. Kohnen T, Herzog M, Hemkeppler E, et al. Visual Performance of a Quadrifocal (Trifocal) Intraocular Lens Following Removal of the Crystalline Lens. *Am J Ophthalmol*. 2017;184:52–62.